Adsorption and 2-Dimensional Association of Lithium Alkyl Dicarbonates on the Graphite Surface through $O^{-}\cdots Li^{+}\cdots\pi$ (arene) Interactions

Yixuan Wang* and Perla B. Balbuena*

Department of Chemical Engineering, Swearingen Engineering Center, University of South Carolina, Columbia, South Carolina 29208

Received: October 18, 2002; In Final Form: January 7, 2003

Adsorptions of several lithium alkyl (vinylene, divinylene, ethylene, and propylene) dicarbonates on the surface of hydrogen-truncated carbon clusters ($C_{54}H_{18}$, $C_{78}H_{20}$, and $C_{96}H_{32}$) are investigated using density functional theory. Lithium alkyl dicarbonates resulting from the reductive decomposition of the respective organic carbonates can be adsorbed on the graphite surface mainly through $O\cdots Li^{+}\cdots\pi$ (arene) interactions, yielding structures with Li^{+} oriented toward the hexane ring center. The adsorption energies of lithium vinylene dicarbonate (LVD), lithium ethylene dicarbonate (LED), and lithium propylene dicarbonate (LPD) on the basal plane of neutral as well as negatively charged $C_{54}H_{18}$, and on the edge plane of the negatively charged $C_{78}H_{22}$, agree within 4.0 kcal/mol, e.g., they are −34.67, −37.40/−35.17 and −38.05 kcal/mol on the basal plane of the negatively charged $C_{54}H_{18}$, respectively; however, the distances from both the carbonyl carbons and alkyl carbons to the nearest graphite carbon clearly increase in the sequence LVD < LED < LPD. In addition, the favorable conformation of LVD is basically parallel to the graphite surface, while those of the latter two dicarbonates are considerably twisted. Adsorption of the trimers for lithium vinylene/ethylene/propylene dicarbonates on the basal plane of $C_{96}H_{22}$ are also discussed. The present results can partially explain several important phenomena occurring in Li-ion batteries.

1. Introduction

The impressive commercial reality of Li-ion batteries raises interest in the science underlying Li-ion battery technology in order to further improve performances and optimize the components of Li-ion batteries (LIBs).[1] Many research efforts have led to the common knowledge that cycle life and stability of lithium-ion rechargeable batteries, consisting of a graphitic carbon anode, a nonaqueous organic electrolyte and a transition metal oxide (such as $LiCoO_2$, $LiMn_2O_4$, and $LiNiO_2$) cathode, are very dependent on the formation of an efficient solid electrolyte interphase (SEI) layer between the graphite anode surface and the electrolyte, which mainly result from the reductive decomposition of the organic carbonate electrolyte during the first several battery charge−discharge cycles. Many studies have been directed toward understanding the mechanism of the reductive decomposition of the electrolyte on the anode surface, and considerable progress has been made on relevant issues, including the identification of the SEI layer leading components as well as the composition of the generated gas. Several hypotheses have been formulated about the SEI generation mechanism.

Nevertheless, two well-known subjects, namely, the failure of propylene carbonate (PC) to build up a proper SEI layer on the graphite surface and the vinylene carbonate (VC) functioning mechanism as an efficient additive for the PC/EC-based solvent, are still not unambiguous and/or controversial explanations exist from different research groups. Despite the close structural similarity between EC and PC, they behave oppositely with respect to the SEI buildup on the graphite anode. Regarding the stable SEI layer formation in EC solution and the destructive reaction behavior occurring in PC solution, Besenhard et al. suggested that the solvent can co-intercalate into the graphite layer to form a ternary graphite intercalation compound (GIC) $[Li(sol)_yC_n]$,[2−4] where the EC decomposition product forms a stable SEI film[3,4] but the products from PC exert a strong interlayer stress in the graphite electrode such that its structure is destroyed.[2,4−6] Another model, originally proposed by Peled et al.[7,8] and further developed by Aurbach et al., [9] raises concerns on the necessity of solvent co-intercalation, stressing that PC is reduced even before its co-intercalation and thus disability of the reduction products to form an effective SEI film leads to the destruction of the graphite electrode. Differences between quantum chemical properties that usually govern redox activities, such as electron affinities (or reduction potentials) and binding energies with Li salt, are not enough to be responsible for the considerable difference.[10] The reduction potentials (with respect to generated reduction intermediates in each case) predicted with cluster-continuum models ($Li^{+}(EC)_2/(PC)_2$−CPCM) are, for example, 1.82 and 1.96 V for PC and EC, respectively. Additionally, except for the presence of a different alkyl group ($-CH_2-CH_2-$ vs $-CH(CH_3)CH_2-$), density functional theory (DFT) calculations indicate that the main products through electro-reductive decomposition, such as lithium alkyl dicarbonate $(ROCO_2Li)_2$, of propylene carbonate (PC) are also similar to those of EC.[10] A question thus arises, i.e., do the adsorptions on the graphite surface of the reduction products from PC and EC differ greatly?

When carbon materials are used as anodes of Li-ion batteries, the addition of a small amount of a highly reactive compound, such as vinylene carbonate (VC),[11,12] to EC/PC-based electrolyte solutions considerably improves the SEI layer in EC solutions

Corresponding authors. E-mail: wangyi@engr.sc.edu. E-mail: balbuena@engr.sc.edu.

10.1021/jp027251+ CCC: $25.00 © 2003 American Chemical Society
Published on Web 05/17/2003

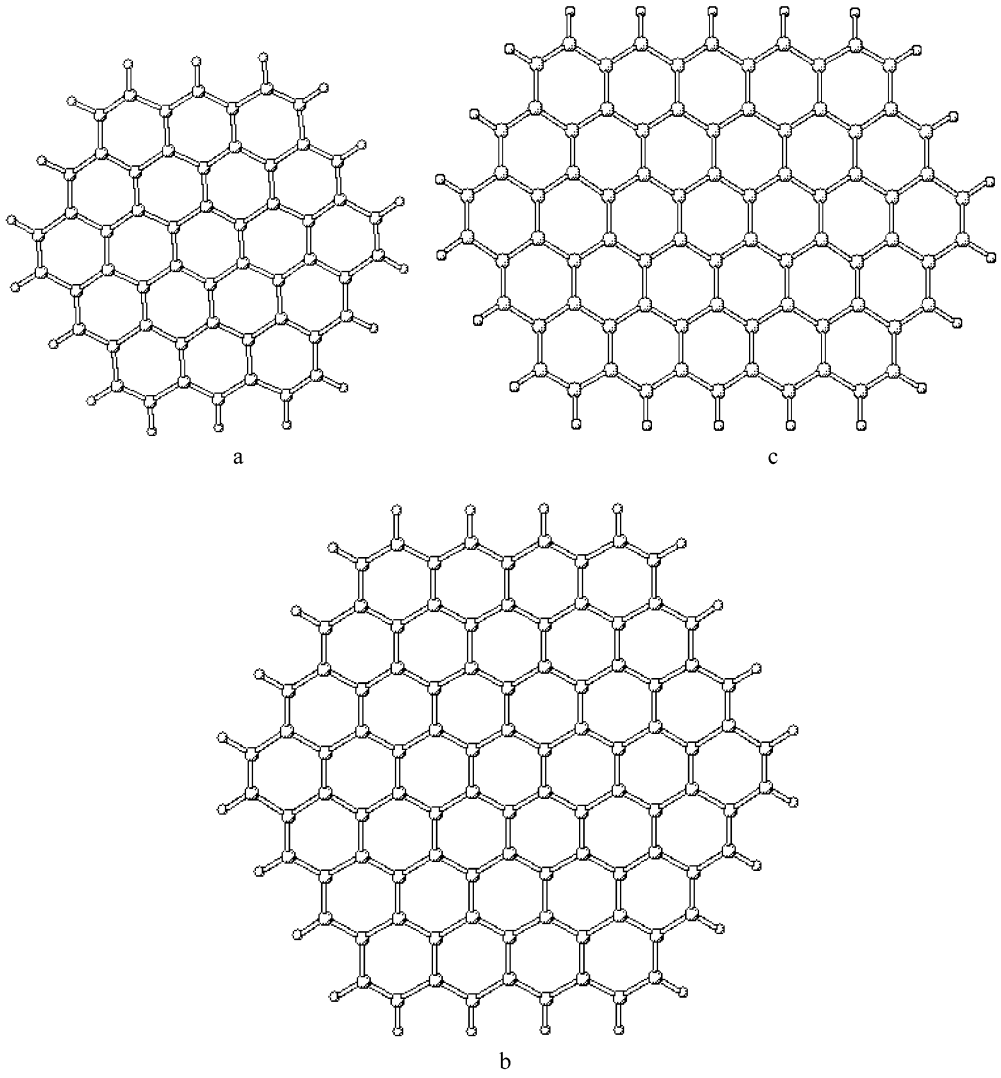

Figure 1. H-truncated graphite models, (a) $C_{54}H_{18}$, (b) $C_{96}H_{24}$, and (c) $C_{78}H_{22}$.

and helps to build up an appropriate SEI in PC solutions. It seems that the VC reduction potential (or electron affinity in the quantum chemistry language) higher than EC and PC, i.e., its preferential reduction on the electrode surface, plays an important role, generating a more stable precursor, which will undergo a homolytic ring opening and eventually will lead to the formation of the SEI layer components. However, the energy barrier for the homolytic ring opening reactions of VC is nearly one time higher than those for EC and PC.[10,13] This implies that the thermodynamics aspects are the ones that dominate the VC role as an electrolyte additive. Regarding the possible main SEI products from VC reduction, $LiOCO_2(CH{=}CH)_nOCO_2Li$ ($n = 1,2$), the significant structural difference is the presence of a double-bond unit, which is suggested as favorable for the SEI formation via polymerization on the electrode surface to generate polymeric or oligomeric species.[14] Provided that an effective adsorption on the graphite surface should occur to form the SEI layer, it is also necessary to investigate whether adsorptions of the unsaturated lithium dicarbonates differ from the saturated ones from EC and PC reductions.

In the present study, DFT is applied to the main reduction products of VC, EC, and PC, focusing upon (i) their adsorption on the edge plane as well as on the basal plane of graphite surface, i.e., equilibrium structures, binding energies, and the effect of the adsorbates on the graphite surface, and (ii) their associations on the graphite surface.

2. Computational Methodology and H-Truncated Cluster Models

2.1. Methods. All the calculations were performed using the G98 program, revision A11.[15] To incorporate possible weak interactions between π bond and π (arene) of graphite surfaces, the Perdew-Wang 1991 exchange functional together with their gradient-corrected correlation functional, denoted as PW91PW91, was used through the present calculations.[16−18] The basis set superposition error (BSSE) corrections were estimated using the counterpoise method of Boys and Bernardi.[19] The charge distributions were characterized by fitting the molecular electrostatic potential to atomic point charges using the CHELPG method.[20]

2.2. H-Terminated Cluster Models. Highly symmetric H-terminated cluster models, $C_{54}H_{18}$ (circumcoronene), $C_{96}H_{24}$, and $C_{78}H_{22}$, are used for simulating graphite surfaces, which are denoted as Gr_{54}, Gr_{96}, and Gr_{78}, respectively. Keeping D_{6h} symmetry and adding 3 and 4 rings around a benzene ring generate the first two (Figures 1a and 1b), which correspond to the series $C_{6n}{}^2H_{6n}$ ($n = 3$ and 4). Removing the top as well as the bottom 9 carbon atoms from $C_{96}H_{24}$ gives rise to the third cluster (Figure 1c) with lower symmetry of C_{2v}. Full optimizations are conducted for $C_{54}H_{18}$ at PW91PW91/3-21G, 4-31G* and 6-31G*. Bond lengths for the inner rings (first and second) C−C are around 1.43 Å and are very close to that (1.42Å) of

TABLE 1: Average Charge (q/e) of Carbons along Successive Circles (n =2, 3, 4) around the Central Ring (n =1) Determined with the CHELPG-PW91PW91 for Neutral Gr_{54}, Gr_{78}, Gr_{96} and the Negative-Charged Gr_{54}^-

	$C_{54}H_{18}$			$C_{54}H_{18}^-$	$C_{94}H_{24}$	$C_{78}H_{22}$
n	3-21G	4-31G*	6-31G*	4-31G*	3-21G	3-21G
1	−0.0005	−0.0048	−0.0018	−0.0159	−0.0055	−0.0017
2	−0.0208	−0.0144	−0.0173	−0.0175	−0.0084	−0.0165
3	−0.0831	−0.0631	−0.0622	−0.0810	−0.0217	−0.0286
4					−0.0729	−0.1025

graphite, while the C−C bonds connecting the peripheral and the second ring are slightly longer, approximately 1.437Å (6-31G*). In the outermost ring, there are three sorts of C−C bonds, 1.372, 1.407, and 1.437Å (6-31G*). In the first, two carbon atoms directly link with a hydrogen atom and behave as double bonds. The results show that C−C bond lengths agree very well within 0.003 Å with the three different basis sets. To keep computation within an acceptable time frame, full optimizations are only performed at 3-21G for the relevant investigations in the two larger clusters. Similarly to $C_{54}H_{18}$, the C−C bonds are in the range of 1.426 to 1.433Å for the three inner rings for $C_{96}H_{24}$, and the lengths of the three kinds of peripheral C−C bonds are 1.369, 1.400, and 1.446 Å, respectively. The diameter of $C_{96}H_{24}$ is approximately 16 Å, being similar to that (20−30 Å) of crystallites in disordered carbon materials prepared by heat treatment of polyphenylene.[21]

The atomization energies per carbon atom (average energy variation for the reaction $C_mH_n \rightarrow mC + nH$) are also calculated to further evaluate the cluster models. They are 196.6, 202.6, and 200.7 kcal/mol for $C_{54}H_{18}$ at PW91PW91/3-21G, 4-31G*, and 6-31G*, respectively, and are further reduced to 193.6 and 191.9 kcal/mol with 3-21G basis set for the larger clusters, $C_{78}H_{22}$ and $C_{96}H_{24}$. This indicates that atomization energies are gently approaching the experimental heat of sublimation of graphite (170.0 kcal/mol at 0 K)[22] as the number of carbons increases.

Table 1 illustrates the influence of the cluster size on charge distributions, showing variations of the average charge of carbons along successive circles (n) around a central one (n = 1). Except for the outermost ring, where carbons directly connecting with hydrogen atoms carry negative charge while others carry positive charge, the charge variations within a circle are not significant. Generally, the average charges for the most inner (central) circle carbons are negative, but rather low, for all the three models, being nearly neutral. Higher negative values are found for the average charge as they are located in the outer circles toward the edges. Moreover, like the C−C bond length, average carbon charges in $C_{54}H_{18}$ do not depend much on the basis sets.

The negatively charged $C_{54}H_{18}$ and $C_{78}H_{22}$ are also fully optimized with PW91PW91/4-31G* and PW91PW91/3-21G, respectively, to incorporate the adsorptions of lithium alkyl dicarbonates on the working graphite anode of LIBs. Graphite has a strong tendency to accept electrons, e.g., the adiabatic electron affinity (EA) of Gr_{54} is 1.3 eV (30.0 kcal/mol), which is defined by the energy difference between the neutral Gr_{54} and the charged Gr_{54}^-. As shown in Table 1, compared with the neutral Gr_{54}, one central carbon (n = 1) gets approximately 0.01 e in Gr_{54}^- (−0.0159 e vs −0.0048 e), the carbons in the second ring (n = 2) change less (−0.0175 e vs −0.0144 e), and consequently the charged electron mainly delocalizes over the edge carbons (−0.54 e) and on the outside hydrogen atoms (−0.34 e).

3. Results and Discussion

3.1. Adsorption of Lithium Alkyl Dicarbonates on the Neutral Graphite Surface. $C_{54}H_{18}$ was initially used to investigate adsorptions of a single molecule on the basal plane of graphite. Adsorption energies (AE), defined by

$$\mathrm{AE} = E(\text{adsorption conformation}) - E(\text{graphite}) - E(\text{lithium alkyl dicarbonate})$$

are summarized in Table 2, and distances from Li^+, carbonyl, as well as alkyl carbons to the nearest graphite carbon are listed in Table 3. Two types of adhesion are located with respect to either parallel or perpendicular orientations of the dicarbonate molecule to the graphite surface. Figures 2a and 2b illustrate the top and side views of lithium vinylene dicarbonate (LVD), $(CHOCO_2Li)_2$, on the surface of $C_{54}H_{18}$, respectively, where

TABLE 2: Total Adsorption Energies (TAE, kcal/mol) and BSSE-Corrected Adsorption Energies (AE, kcal/mol) of Lithium Alkylene Dicarbonates on Neutral and Charged Graphite Surfaces with PW91PW91 Method

		3-21G			4-31G*			6-31G*		
conf[a]	individual components	TAE[b]	BSSE	AE	TAE	BSSE	AE	TAE	BSSE	AE
1	LVD+Gr_{54}	−38.84	31.09	−7.75	−23.27	10.94	−12.33	−21.19	9.10	−12.12
2	LVD+Gr_{54}	−40.34	29.98	−10.36	−21.71	10.42	−11.30			
1(78)	LVD+Gr_{78}	−38.90								
3	LDVD+Gr_{54}	−36.91	27.72	−9.19	−23.83					
3(78)	LDVD+Gr_{78}	−40.16	33.61	−6.55						
4	LED+Gr_{54}	−41.70	28.96	−12.74	−25.29	10.53	−14.76	−23.46	8.53	−14.93
5	LED+Gr_{54}	−40.13	30.94	−9.19	−23.68	10.95	−12.73	−21.47	8.92	−12.55
4(78)	LED+Gr_{78}	−41.46								
6	LPD+Gr_{54}	−40.97	26.08	−14.89	−25.75	10.40	−15.35	−23.44	8.39	−15.05
7	LPD+Gr_{54}	−39.97	30.04	−9.93						
7(78)	LPD+Gr_{78}	−39.56								
8	LVD+Gr_{54}^-				−34.67					
9	LED+Gr_{54}^-				−37.40	10.62				
10	LED+Gr_{54}^-				−35.17	11.39				
11	LPD+Gr_{54}^-				−38.05					
12	LVD+Gr_{78}^-	−40.92								
13	LED+Gr_{78}^-	−41.81								
14	LPD+Gr_{78}^-	−44.57								

[a] **1**(**78**) and others with parentheses refer to the corresponding conformations on $C_{78}H_{22}$. [b] TAE= E(conformations) − E(lithium alkylene dicarbonate) − E(graphite); AE=TAE + BSSE.

TABLE 3: The Distance (Å) from Lithium, Carbonyl Carbon (C1 and C4), and Alkyl Carbon (C2 and C3) of Lithium Alkylene Dicarbonates to the Nearest Graphite Carbon

	conf.											
	1 LVD $+Gr_{54}$	**2** LVD $+Gr_{54}$	**4** LED $+Gr_{54}$	**5** LED $+Gr_{54}$	**6** LPD $+Gr_{54}$	**8** LVD $+Gr_{54}^-$	**9** LED $+Gr_{54}^-$	**10** LED $+Gr_{54}^-$	**11** LPD $+Gr_{54}^-$	**12** LVD $+Gr_{78}^-$	**13** LED $+Gr_{78}^-$	**14** LPD $+Gr_{78}^-$
						3-21G						
Li1	2.436	2.336	2.287	2.392	2.254					2.32	2.33	2.27
C1	3.530	3.730	4.189	3.688	4.232					3.57	3.57	3.79
C2	4.059	4.630	5.383	4.453	5.553					4.30	4.33	4.66
C3	4.019	4.164	4.540	4.315	4.986					4.25	4.50	4.84
C4	3.526	3.582	3.731	3.647	4.049					3.82	3.84	4.00
Li2	2.441	2.469	2.419	2.383	2.264					2.42	2.46	2.34
						4-31G*						
Li1	2.589	2.489	2.459	2.535	2.606	2.526	2.500	2.479	2.466			
C1	3.665	4.134	4.328	3.853	4.206	3.793	4.244	4.022	4.297			
C2	4.209	5.241	5.389	4.619	5.492	4.433	5.591	4.949	5.676			
C3	4.212	4.463	4.625	4.633	4.953	4.430	4.879	4.759	5.043			
C4	3.666	3.845	3.843	3.859	3.989	3.796	4.041	3.981	4.060			
Li2	2.589	2.546	2.611	2.534	2.444	2.526	2.651	2.465	2.415			
						6-34G*						
Li1	2.591		2.601	2.542	2.614							
C1	3.681		4.328	3.857	4.214							
C2	4.235		5.389	4.625	5.507							
C3	4.234		4.625	4.634	4.974							
C4	3.681		3.843	3.860	4.000							
Li2	2.590		2.611	2.542	2.454							

LVD is located nearly parallel to the graphite surface (conformation **1**). Figure 2a clearly shows that the two Li^+ gravitate around the C_6 ring center with η^6-coordination, in which the separations of Li^+ to the two inner carbons are approximately 0.10−0.15Å shorter than those to the other four carbon atoms. From Figure 2b, lithium vinylene dicarbonate significantly bends toward the graphite surface, perhaps as a result of the strong interactions between Li^+ and arene π, denoted as $O^-\cdots Li^+\cdots\pi$ (arene).

Figure 2b also shows that the distances from LVD atoms to the nearest graphite C atoms, predicted by PW91PW91/6-31G*, are only slightly longer by less than 0.03 Å than those obtained using PW91PW91/4-31G*. Consequently, the adsorption energies only differ by 0.20 kcal/mol (−12.12 vs −12.33 kcal/mol). However, PW91PW91/3-21G significantly underestimates the distances by 0.15 −0.20 Å. The deficiency of the smallest basis set 3-21G is also reflected by the adsorption energies summarized in Table 2, which are considerably overestimated at the 3-21G basis set, where the BSSE is even two times higher than adsorption energy itself.

Starting from a geometry perpendicular to the graphite surface, another stationary point—conformation **2**—is located. As illustrated in Figure 3, the LVD molecule basically remains in its planar structure, whereas the dihedral between the LVD molecular plane and the graphite surface is much less than 90°. Again, considerable shorter separations and higher adsorption energy arise from the 3-21G basis set. Since the distances between the end Li^+ and the nearest graphite carbon atoms, predicted with 4-31G* for conformations **2** and **1**, agree within 0.1 Å, but those of carbonyl C as well as alkyl C of **2** are much farther than those of **1**, the adsorption energy difference of 1.0 kcal/mol may be mainly attributed to the interaction between the π(double bond) of LVD and the π(arene) of graphite, which is stronger in conformation **1** than in **2** as a result of the favorable geometry of the former.

The adsorption of lithium ethylene dicarbonate (LED) on the surface of $C_{54}H_{18}$ has a pattern similar to LVD, viz., arched LED as shown in Figure 4 (conformation **4**, and **5**), which correspond to the perpendicular and parallel adsorptions of LED,

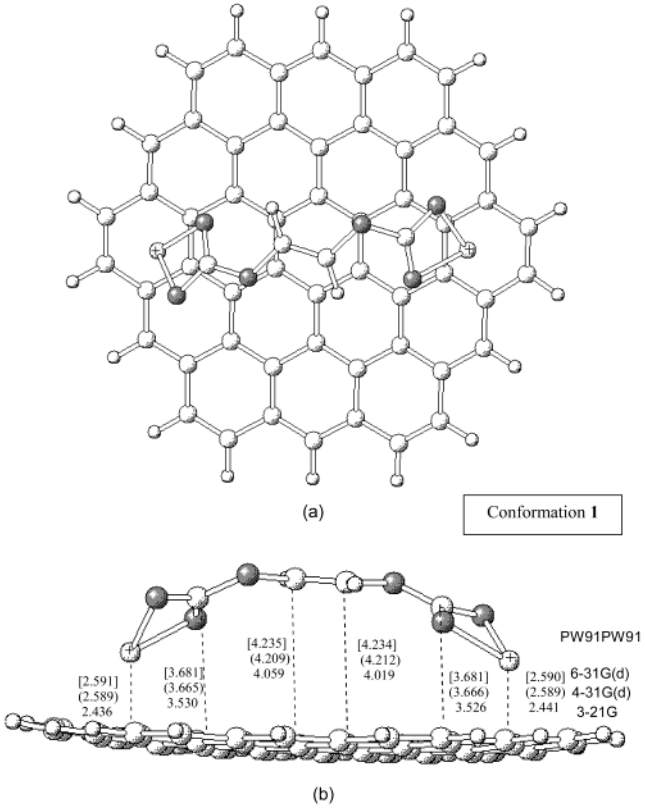

Figure 2. Adsorptions of lithium vinylene dicarbonate on the surface of $C_{54}H_{18}$. Solid balls stand for oxygen atoms, big empty ones for carbon atoms, small empty ones for hydrogen atoms, and the balls marked with a star stand for lithium atoms. The numbers refer to the distances between LVD atoms and the nearest graphite carbons: those in brackets, in parentheses, and outside are from PW91PW91/6-31G*, PW91PW91/4-31G*, and PW91PW91/3-21G, respectively. (a) Top view, and (b) side view of conformation **1**. The corresponding distances for the parallel conformation **1(78)** on $C_{78}H_{22}$ are 2.437, 3.458, 3.906, 3.908, 3.457, and 2.436 Å.

respectively. In contrast to the LVD case, the perpendicular adsorption conformation **4** is more stable, by approximately 2.0

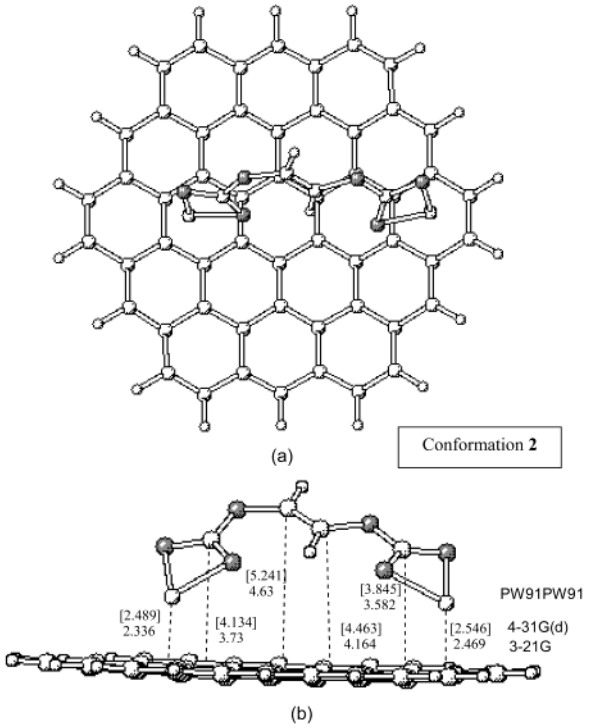

Figure 3. Perpendicular adsorption of lithium vinylene dicarbonate on the surface of $C_{54}H_{18}$. (a) Top view, (b) side view of conformation **2**. The numbers have the same meanings as in Figure 2.

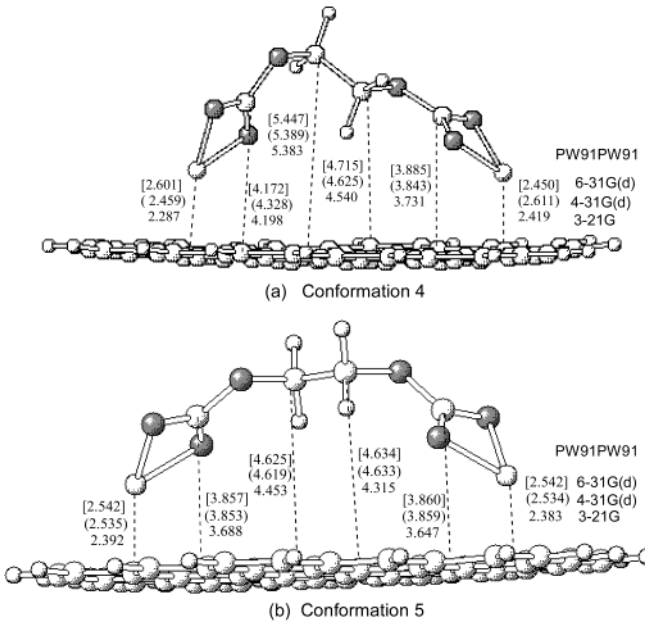

Figure 4. Side views of the adsorption of lithium ethylene dicarbonate on the surface of $C_{54}H_{18}$: (a) conformation **4**, (b) conformation **5**. The numbers have the same meanings as in Figure 2. The corresponding distances for the perpendicular conformation on $C_{78}H_{22}$ are 2.473, 3.994, 5.235, 4.320, 3.651, and 2.257 Å.

kcal/mol, than the parallel conformation **5** (AE: −14.76 vs −12.73 kcal/mol and −14.93 vs −12.55 kcal/mol at PW91PW91/4-31G* and 6-31G*, respectively). This may be a result of less repulsion between the ($-C_2H_4-$) group and graphite in **4** than in **5**. Comparing the parallel adsorption conformations **1** and **5**, although the average distances from Li to the nearest-neighbor graphite C atoms are around 2.5 Å at 4-31G* for both cases, the shortest distances from carbonyl as well as ethylene carbons to graphite carbon are longer by approximately 0.18 and 0.42

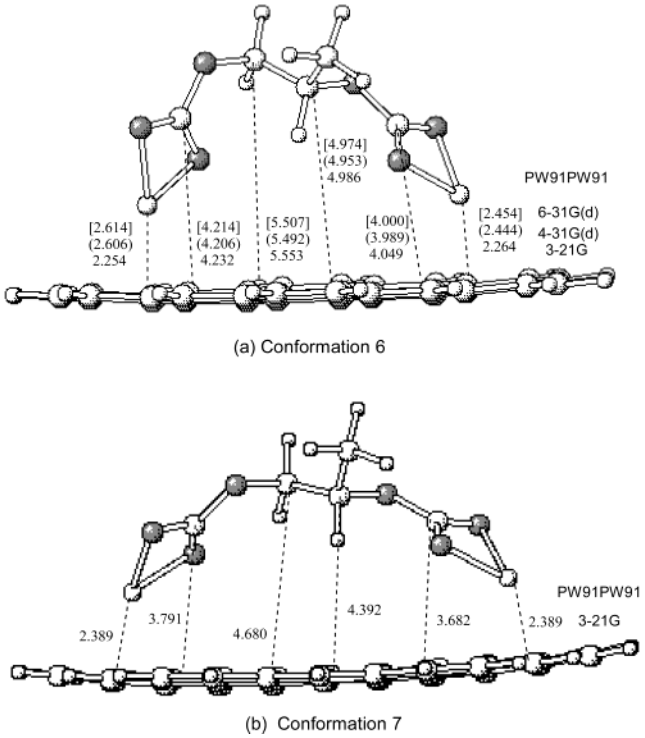

Figure 5. Side views of the adsorption of lithium propylene dicarbonate on the surface of $C_{54}H_{18}$: (a) conformation **6**, (b) conformation **7**. The numbers have the same meanings as in Figure 2. The corresponding distances for conformation (a) on $C_{78}H_{22}$ are 2.414, 3.689, 4.475, 4.281, 3.623 and 2.398 Å.

Å than the corresponding ones of LVD (*R*: 3.85 vs 3.67Å, 4.62 vs 4.21 Å), which means that the adsorption of LED is not as compact as that of LVD. A similar conclusion could also be reached by comparison between the perpendicular conformations **4** and **2** (*R*: 4.328, 3.843, 5.389, 4.625 Å vs 4.134, 3.845, 5.241, 4.463 Å at PW91PW91/4-31G*). The comparison between the favorable conformations, i.e., **1** of LVC and **4** of LED, shows that such differences become considerably larger (4.328, 3.843, 5.389, 4.625 Å vs 3.853, 3.859, 4.619, 4.633 Å).

Regarding lithium propylene dicarbonate (LPD), both the corresponding parallel and perpendicular adsorption conformations were indeed located at the PW91PW91/3-21G level, as shown in Figure 5. Conformation **7** does not keep symmetry anymore because of the methyl group, where the propylene carbon connecting with the methyl group has a shorter distance (4.392 vs 4.680 Å at PW91PW91/3-21G) to the graphite surface than the other one does. However, only favorable conformation **6** was found at the two higher levels. In conformation **6** the distances from the carbonyl carbons to the nearest graphite carbon are longer, by 0.04 and 0.11 Å, than those in conformation **4** (*R*: 4.214, 4.000 Å vs 4.172, 3.885 Å at 6-31G*), *R* for alkyl carbons are also further increased by approximately 0.10 and 0.32 Å (5.507, 4.974 Å vs 5.426, 4.657). The results imply that the adsorption of LPD becomes looser than that of lithium ethylene dicarbonate. It is noted that the small basis set 3-21G considerably underestimates (overestimates) *R* (adsorption energies before BSSE); however, it qualitatively provides similar trends to 4-31G* and 6-31G* about adsorptions of the three lithium dicarbonates. In the following section, the 3-21G basis set is used for the $C_{96}H_{24}$ surface.

Single molecular adsorptions on the neutral graphite show that the favorable conformation of LVD from VC reduction is parallel as well as nearer (as shown in Table 3) to the graphite surface, whereas one end turns upward from the surface of those

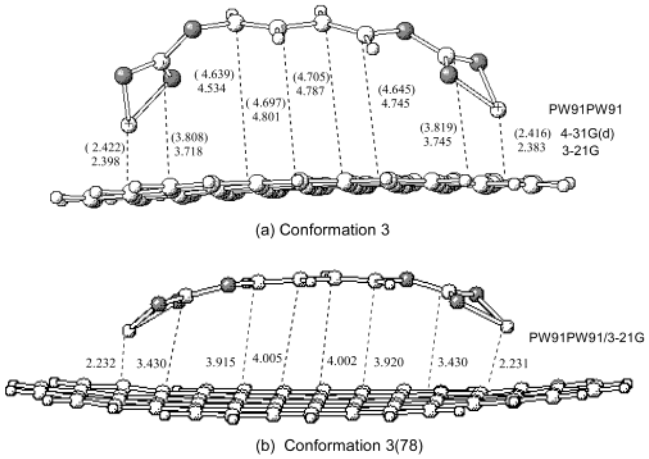

Figure 6. Adsorption of lithium divinylene dicarbonate on the graphite surfaces of $C_{54}H_{18}$ and $C_{78}H_{22}$: (a) conformation **3,** (b) conformation **3**(78).

of LED and LPD, especially the latter one. The adsorption energies of LED and LPD are very similar (−14.9 vs −15.1 kcal/mol), and they are 2−3 kcal/mol more negative than that of LVD. We therefore speculate that the compactness may be responsible for the passivation ability of the graphite anode, and ultimately about the performance of rechargeable Li-ion batteries. Thus, Li-ion batteries can perform well when VC is present in the electrolyte because the main product from the VC decomposition could form a more compact layer on the graphite surface; on the other hand, a loose layer is expected from VC-free electrolytes, especially PC-based electrolyte, leading to bad performances of Li-ion batteries.

The parallel adsorption (conformation **3**) of lithium divinylene dicarbonate (LDVD) is also investigated using both $C_{54}H_{18}$ and $C_{78}H_{22}$ clusters, the respective side views are illustrated in Figure 6. Except for the two Li^+, the carbonyl carbon atoms as well as the alkyl carbons separate from the $C_{54}H_{18}$ surface much more than they do in Figure 1b (averaged *R* of carbonyl and alkyl carbons: 3.82, 4.67 Å vs 3.67, 4.21 Å at PW91PW91/4-31G*). However, the distances of LDVD to $C_{78}H_{22}$ are considerably reduced, and they are even slightly shorter by approximately 0.1 Å than those of LVD. However, the adsorptions of LVD, LED, and LPD on $C_{78}H_{22}$, with *R* values given, respectively, in Figures 2b, 4b, and 5b, are similar to those on $C_{54}H_{18}$ both regarding *R* and the adsorption energies. This means that the $C_{54}H_{18}$ model is not big enough to represent adsorption of LDVD but is suitable for LVD, LED, and LPD.

3.2. Adsorption of Lithium Alkyl Dicarbonates on the Negatively Charged Graphite Surfaces (Gr_{54}^- and Gr_{78}^-). Adsorption of LVD, LED, and LPD on the charged graphite surface (Gr_{54}^-) (conformations **8**, **9**, **10**, and **11**), which correspond to conformations of **1**, **4**, **5**, and **7** of their adsorption on the neutral surface Gr_{54}, are also investigated in order to incorporate adsorption on the negatively charged anode basal plane. Similarly, their adsorption energies do not differ much either (TAE, LVD: −34.67; LED: −37.40 and −35.17; LPD: −38.05). As in the case of their adsorption on the neutral basal plane Gr_{54}, Table 3 shows that both the carbonyl carbon atoms and alkyl carbon atoms of LVD (conformation **8**) have significantly shorter distances to the nearest graphite carbons than those of LED (conformations **9** and **10**) (C1, C2, C3, and C4, conformation **8**: 3.793, 4.433, 4.430, and 3.796 Å; conformation **9**: 4.244, 5.591, 4.879, and 4.041 Å; conformation **10**: 4.022, 4.949, 4.759, and 3.981 Å). In turn, conformation **11** of LPD adsorption has an even longer distance than that of conformation **9** of LED adsorption. The averaged distance to the nearest graphite carbon in conformation **8** is shorter by 0.31 Å, 0.58 Å, and 0.66Å than those in conformation **10**, **9**, and **11**, respectively.

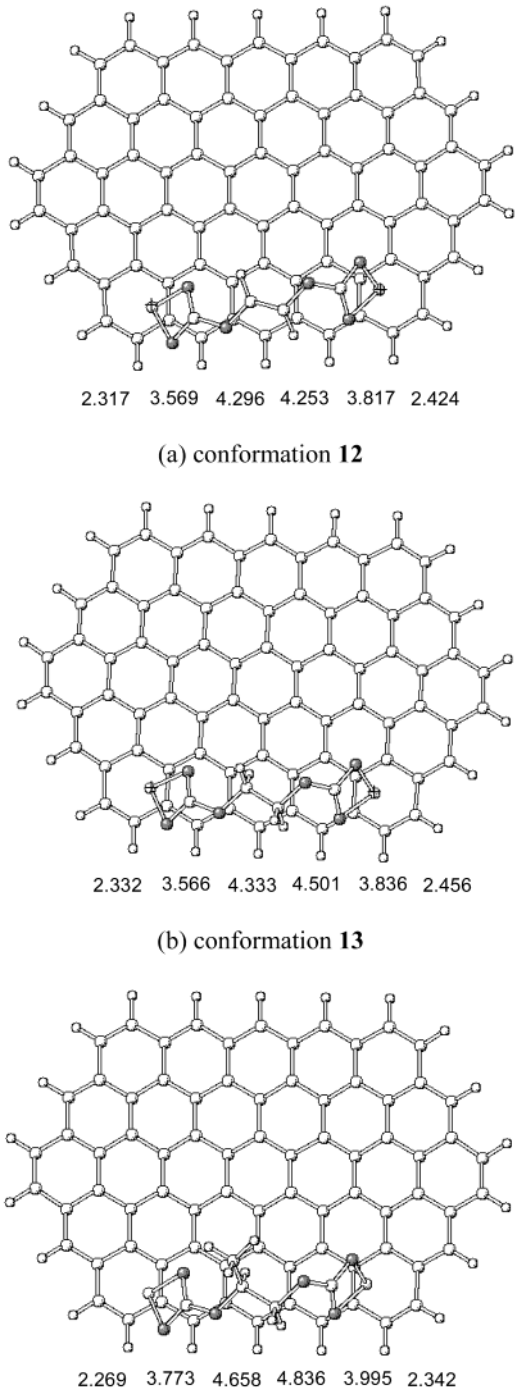

Figure 7. Top views of adsorptions on the negatively charged $C_{78}H_{22}$ of LVD (a) conformation **12**, LED (b) conformation **13** and LPD conformation **14**.

Top views for adsorption of the three lithium alkyl dicarbonates on the edge plane of the negatively charged graphite, Gr_{78}^-, are illustrated in Figure 7. It is well recognized that the reactivity of zigzag and armchair carbons in the edges is much different from that of the carbons in the graphite basal plane, which is reflected by the rather different charge distribution among $C_{54}H_{18}^-$ shown in Table 1 and may affect the reductive

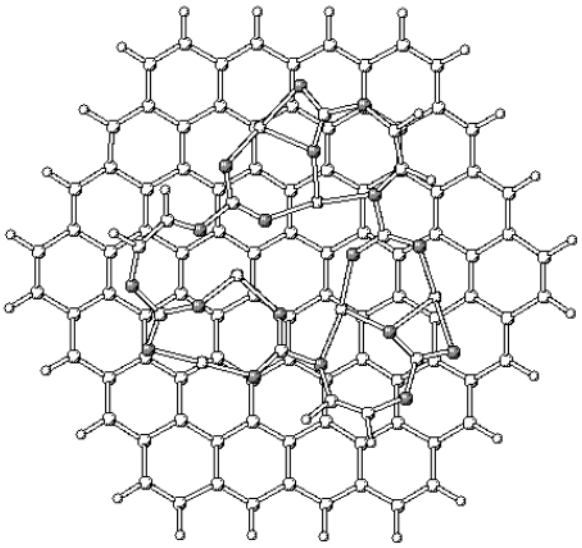

Figure 8. Top view of adsorption of lithium vinylene dicarbonate trimer on $C_{96}H_{24}$ surface.

decomposition of organic carbonates and the successive adhesion of the decomposition products. The total adsorption energies (TAE) of LVD, LED, and LPD on the edge of Gr_{78}^- also agree within 4 kcal/mol (TAE: LVD, −40.92; LED, −41.81; LPD, −44.57 kcal/mol). The averaged distance to the nearest graphite carbon has the same sequence as for the basal plane of Gr_{54}^-; however, the difference becomes smaller, e.g., the averaged distances in conformation **12** (LVD + Gr_{78}^-), conformation **13** (LED + Gr_{78}^-), and conformation **14** (LPD + Gr_{78}^-) are 3.98, 4.06, and 4.32 Å, respectively. Thus, it may be safe to conclude that LVD, the main product from VC reduction, forms the most compact layer on the basal plane as well as the edge plane of the charged graphite anode, followed by LED, the product of EC, and the least is LPD from PC reduction.

3.3. 2-Dimensional Association of Lithium Alkyl Dicarbonates on the Graphite Surface (Gr_{96}). Lithium alkyl dicarbonate can strongly associate through $O^-\cdots Li^+\cdots O^-$ interactions, and can grow adopting the closed structure conformation, that is, they associate to the cage-like dimer first, then to the closed pseudo-planar trimer, to the closed tetramer, and so on.[23] As illustrated in Figure 8, $C_{96}H_{24}$ is an adequate model for adsorption of the pseudo-planar trimer of Li alkyl dicarbonates. Associations of lithium alkyl dicarbonates reduce the interactions of Li^+ with the cluster surface, which is demonstrated by longer distances between Li^+ and its nearest-neighbor graphite carbons (*R* is approximately 0.5 Å larger than the monomer). Consequently, trimers may exist in pseudo-planar geometries above the graphite surface, as shown in Figure 9, rather than in an arched geometry like a single molecule. Moreover, adsorption energies are only 10∼20 kcal/mol higher than those of monomers (BSSE- free AE: 47.9, 51.7, 54.5 kcal/mol vs 38.9, 41.7, 41.0 kcal/mol at PW91PW91/3-21G).

Similarly to single molecular adsorptions, the trimer of lithium vinylene dicarbonate basically is parallel to the graphite surface (Figure 9a), while one of alkyl (ethylene and propylene) carbons turns upward from graphite surfaces. The distances from carbonyl and vinylene carbons of lithium vinylene dicarbonate to the nearest graphite carbons are again shorter than the corresponding distances of lithium ethylene dicarbonate and lithium propylene dicarbonate. This result also indicates that the monolayer from lithium vinylene dicarbonate is more compact than those from the other two saturated dicarbonates, which may have a positive impact on the SEI layer buildup.

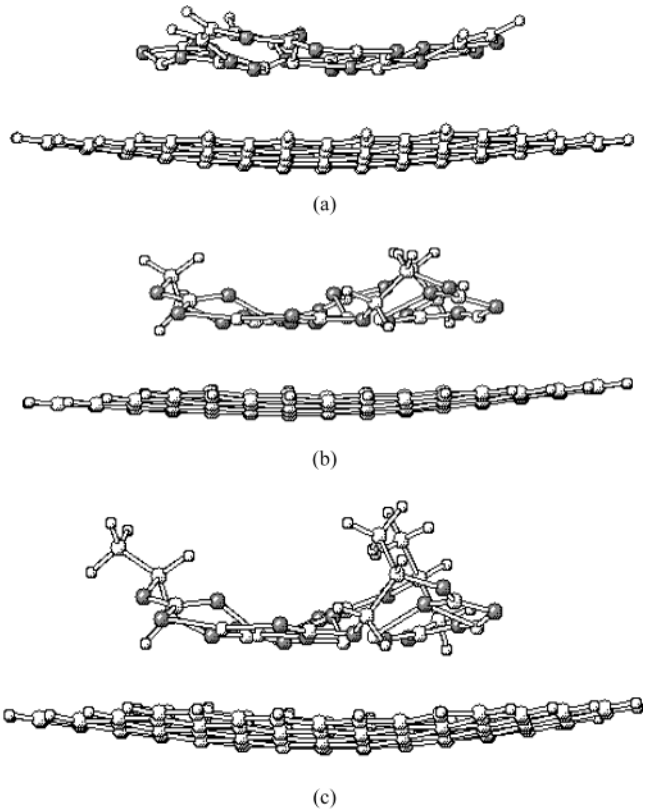

Figure 9. Side views of adsorptions on $C_{96}H_{24}$ (a) lithium vinylene dicarbonate trimer, (b) lithium ethylene dicarbonate trimer, (c) lithium propylene dicarbonate trimer.

It is interesting to note that the graphite surface in Figure 9c twists more than those of Figures 9a and 9b do. This may be responsible for the failure behavior of graphite in PC-based electrolytes. Additionally, although the distances to the graphite surfaces for LED and LPD trimers are not as much different as those of their monomers, the upward methyl group probably affects the 3-dimensional associations of lithium propylene dicarbonate, which suggests that multilayer SEI buildup in PC-based electrolytes is not as favorable as those in EC-based as well as VC-containing electrolytes.

4. Conclusions

Adsorption of several lithium alkyl (vinylene, divinylene, ethylene, and propylene) dicarbonates and their trimers on the basal plane ($C_{54}H_{18}$, $C_{78}H_{20}$, and $C_{96}H_{32}$) as well as on the edge plane ($C_{78}H_{22}$) of hydrogen-truncated carbon clusters were extensively studied with density functional theory. Regarding the methods employed, although PW91PW91/3-21G overestimates (underestimates) the adsorption energies (distances to the cluster surface), it provides comparable trends with the other two higher-level methods, PW91PW91/4-31G* and PW91PW91/6-31G*, for the adsorption of lithium alkyl dicarbonates.

The adsorption energies of LVD, LED, and LPD on the basal plane of neutral as well as that of the negatively charged $C_{54}H_{18}$, and on the edge plane of the negatively charged $C_{78}H_{22}$, agree within 4.0 kcal/mol, e.g., they are −34.67, −37.40/-35.17, and −38.05 kcal/mol on the basal plane of the charged $C_{54}H_{18}$, respectively; however, their adsorption patterns are considerably different. First, the most favorable adsorption conformations on the basal plane for both the monomer and trimer of LVD are basically parallel to the graphite surface, while the corresponding adsorptions clearly result in distortions for LED and LPD, with one alkyl carbon turning upward, particularly for LPD. Such

difference may further affect the 3-dimensional growth of the SEI layer. Second, the adsorption of LVD is more compactly attached to the graphite surface than those of lithium ethylene/propylene dicarbonate. Additionally, the adsorption of LPD trimer results in significant deformation of the graphite surface, whereas it remains almost planar for the adsorptions of LVD/LED.

Overall, LVD from VC reductive decomposition could form a parallel and compact layer on the basal plane and the edge plane of graphite surface, whereas LED/LPD from EC/PC reductions results in a loose layer and LPD also may seriously deform the graphite surface. This difference probably is one of the main reasons why a small amount of VC in EC/PC-based can improve the buildup of the SEI layer, and why the reduction product of PC cannot form an effective SEI layer. Taking into account the SEI formation between graphite layers, the loose adsorption and the steric effect of the methyl group may strongly stress the graphite structure, causing its destruction. Other factors which also could be responsible for graphite destruction in PC solutions, such as propylene gas arising from solvent reduction,[24] will be discussed in a separate paper.

Acknowledgment. This work was partially supported by NSF (Career Award Grant CTS-9876065 to P.B.B.), and by Mitsubishi Chemical Corporation. Discussions with Prof. Aurbach are appreciated.

References and Notes

(1) Tarascon, J.-M.; Armand, M. *Nature* **2001**, *414*, 359.
(2) Besenhard, J. O.; Fritz, H. P. *J. Electrochem. Soc.* **1974**, *3*, 329.
(3) Besenhard, J. O.; Winter, M.; Yang, J.; Biberacher, W. *J. Power Sources* **1995**, *54*, 228.
(4) Winter, M.; Besenhard, J. O. In *Lithium Ion Batteries: Fundamentals and Performances*; Wakihara, M., Yamamoto, O., Eds.; Wiley-VCH: New York, 1999; p 127.
(5) Jeong, S.-K.; Inaba, M.; Abe, T.; Ogumi, Z. *J. Electrochem. Soc.* **2001**, *148*, A989.
(6) Chung, G.-C.; Kim, H.-J.; Yu, S.-I.; Jun, S.-H.; Choi, J.-W.; Kim, M.-H. *J. Electrochem. Soc.* **2000**, *147*, 4391.
(7) Peled, E. Lithium Stability and Film Formation in Organic and Inorganic Electrolyte for Lithium Battery Systems. In *Lithium Batteries*; Gabano, J. P., Ed.; Academic Press: New York, 1983.
(8) Peled, E.; Golodnitsky, D.; Menachem, C.; Bar-Tow, D. *J. Electrochem. Soc.* **1998**, *145*, 3482.
(9) Aurbach, D.; Levi, M. D.; Levi, E.; Schechter, A. *J. Phys. Chem. B* **1997**, *101*, 2195.
(10) Wang, Y. X.; Balbuena, P. B. *J. Phys. Chem. B* **2002**, *106*, 4486.
(11) Jehoulet, C.; Biensan, P.; Bodet, J. M.; Broussely, M.; Tessier-Lescourret, C. Batteries for Portable Applications and Electric Vehicles. *The Electrochemical Society Proceedings Series*, 1997, Pennington, NJ.
(12) Fujimoto, M.; Shouji, Y.; Nohma, T.; Nishio, K. *Denki Kagaku* **1997**, *65*, 949.
(13) Wang, Y. X.; Nakamura, S.; Tasaki, K.; Balbuena, P. B. *J. Am. Chem. Soc.* **2002**, *124*, 4408.
(14) Aurbach, D.; Gamolsky, K.; Markovsky, B.; Gofer, Y.; Schmidt, M.; Heider, U. *Electrochim Acta* **2002**, *47*, 1423.
(15) Frisch, M. J.; Trucks, G. W.; Schlegel, H. B.; Scuseria, G. E.; Robb, M. A.; Cheeseman, J. R.; Zakrzewski, V. G.; Montgomery, J. A.; Stratmann, R. E.; Burant, J. C.; Dapprich, S.; Millam, J. M.; Daniels, A. D.; Kudin, K. N.; Strain, O. F. M. C.; Tomasi, J.; Barone, B.; Cossi, M.; Cammi, R.; Mennucci, B.; Pomelli, C.; Adamo, C.; Clifford, S.; Ochterski, J.; Petersson, G. A.; Ayala, P. Y.; Cui, Q.; Morokuma, K.; Malick, D. K.; Rabuck, A. D.; Raghavachari, K.; Foresman, J. B.; Ciolovski, J.; Ortiz, J. V.; Stefanov, V. V.; Liu, G.; Liashensko, A.; Piskorz, P.; Komaroni, I.; Gomperts, R.; Martin, R. L.; Fox, D. J.; Keith, T.; Al-Laham, M. A.; Peng, C. Y.; Nanayakkara, A.; Gonzalez, C.; Challacombe, M.; Gill, P. M. W.; Johnson, B.; Chen, W.; Wong, M. W.; Andres, J. L.; Head-Gordon, M.; Replogle, E. S.; Pople, J. A. *GAUSSIAN 98*, Revision A.9; Gaussian Inc.: Pittsburgh, PA, 1998.
(16) Perdew, J. P. Unified theory of exchange and correlation beyond the local density approximation. In *Electronic Structure of Solids*; Ziesche, P., Eschrig, H., Eds.; Akademie Verlag: Berlin, 1991.
(17) Burke, K.; Perdew, J. P.; Wang, Y. *Electronic Density Functional Theory: Recent Progress and New Directions*; Plenum: New York, 1998.
(18) Perdew, J. P.; Burke, K.; Wang, Y. *Phys. Rev. B* **1996**, *54*, 16533.
(19) Boys, S. F.; Bernardi, F. *Mol. Phys.* **1970**, *19*, 553.
(20) Breneman, C. M.; Wiberg, K. B. *J. Comput. Chem.* **1990**, *11*, 361.
(21) Patric, J. W. *Porosity in Carbons*; Edward Arnold: London, 1995.
(22) Lias, S. G.; Bartmess, J. E.; Liebman, J. F.; Holmes, J. L.; Levin, R. D.; Mallard, W. G. *J. Phys. Chem. Ref. Data* **1988**, *17 (Suppl. 1)*.
(23) Wang, Y. X.; Balbuena, P. B. *J. Phys. Chem. A* **2002**, *106*, 9582.
(24) Aurbach, D. Private communication, 2002.